BIOCHEMISTRY
including biophysical chemistry & molecular biology

ARTICLE

pubs.acs.org/biochemistry

# Combined Structural and Functional Investigation of a C-3″-Ketoreductase Involved in the Biosynthesis of dTDP-L-Digitoxose

Rachel L. Kubiak and Hazel M. Holden*

Department of Biochemistry, University of Wisconsin, Madison, Wisconsin 53706, United States

**ABSTRACT:** L-Digitoxose is an unusual dideoxysugar found attached to various pharmacologically active natural products, including the antitumor antibiotic tetrocarcin A and the antibiotics kijanimicin and jadomycin B. Six enzymes are required for its production starting from glucose 1-phosphate. Here we describe a combined structural and functional investigation of KijD10, an NADPH-dependent C-3″-ketoreductase that catalyzes the third step of L-digitoxose biosynthesis in the African soil-dwelling bacterium *Actinomadura kijaniata*. KijD10 belongs to the glucose-fructose oxidoreductase superfamily. For this investigation, both binary and ternary complexes of KijD10 were crystallized, and their structures were determined to 2.0 Å resolution or better. On the basis of these high-resolution structures, two potential active site acids were identified, Lys 102 and Tyr 186. These residues were individually mutated and the resultant proteins investigated both kinetically and structurally. The Y186F mutant protein demonstrated significant catalytic activity, and its structure was virtually identical to that of the wild-type enzyme except for the positioning of the nicotinamide ring. All lysine mutations, on the other hand, resulted in proteins with either abolished or drastically reduced catalytic activities. Structures for the K102A and K102E mutant proteins were determined and showed that the abrogation of catalytic activity was not a result of large conformational changes. Taken together, these data suggest that Lys 102 donates a proton to the C-3″ keto group during the reaction and that Tyr 186 serves only an auxiliary role. This is in contrast to that proposed for glucose-fructose oxidoreductase and other family members in which the tyrosines, or in some cases similarly positioned histidines, are thought to play major catalytic roles.

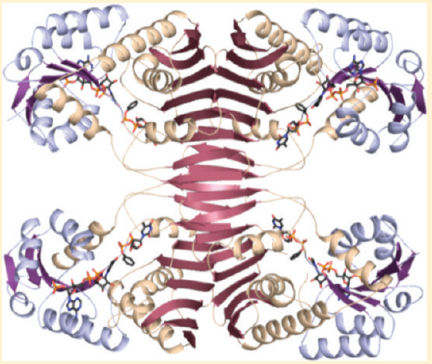

It has become increasingly apparent within the past decade that the unusual di-, tri-, and tetradeoxysugars found throughout nature play critical roles in such diverse processes as the immune response and drug efficacy.[1,2] One of these novel dideoxysugars is L-digitoxose, which is found attached to the antitumor antibiotics referred to as tetrocarcins. The tetrocarcins were first identified from a broth culture of *Micromonospora chalcea* in 1980,[3] and it has since been shown that their antibacterial activities are directly proportional to the number of deoxysugars attached to their aglycone rings.[4] Tetrocarcin A induces apoptosis in human breast cancer cells and thus could prove to be useful as a new chemotherapeutic agent.[5] Besides the tetrocarcins, L-digitoxose has also been observed attached, for example, to the antibiotic kijanimicin,[6] to various antifungal antibiotics,[7] and to jadomycin B, a compound that demonstrates antibacterial activity against methicillin-resistant *Staphylococcus aureus*.[8]

The biosynthetic pathway for the production of L-digitoxose in the soil-dwelling bacterium *Actinomadura kijaniata* is shown in Scheme 1. Six enzymes are required for this bacterium to convert glucose 1-phosphate to dTDP-L-digitoxose.[6,9] The first two steps, the attachment of a nucleotide monophosphate to glucose 1-phosphate and the subsequent dehydration of the sugar ring, are common to many of the pathways for the production of unusual sugars.[10,11] Following these initial reactions, the next step involves the removal of the sugar C-2″ hydroxyl group and the generation of a ketone moiety at C-3″ by a 2,3-dehydratase known as KijB1. Subsequently, the C-3″ keto moiety is reduced by the action of KijD10. An epimerization about C-5″ by KijD11 occurs in the penultimate step of the pathway, and finally, the C-4″ keto moiety is reduced to a hydroxyl by the action of KijC2.

The focus of this combined structural and functional investigation is on KijD10 (highlighted in gray in Scheme 1). It is an NADPH-dependent dehydrogenase containing 332 amino acid residues per subunit. On the basis of amino acid sequence homology, KijD10 is known to belong to the glucose-fructose oxidoreductase (GFOR) superfamily.[12] Members of this superfamily display distinctly bilobal subunit architectures with the N-terminal domains containing Rossmann folds and the C-terminal domains consisting primarily of mixed "open-faced" $\beta$-sheets. Monomeric, dimeric, and tetrameric quaternary structures of proteins belonging to the GFOR superfamily have been observed, and recently, one member has been shown to function as an octamer.[13] Interestingly, Gal80p, a member of the superfamily, functions not as an enzyme but as a dimeric transcriptional inhibitor.[14]

For this investigation, we determined the high-resolution structure of KijD10 in complex with $NADP^+$ and dTDP-benzene, a substrate analog. In addition, various site-directed mutant proteins were prepared to test the roles of Lys 102 and Tyr 186 in catalysis. Both the structures and the kinetic parameters for

**Received:** April 5, 2011
**Revised:** May 18, 2011
**Published:** May 20, 2011

**Scheme 1**

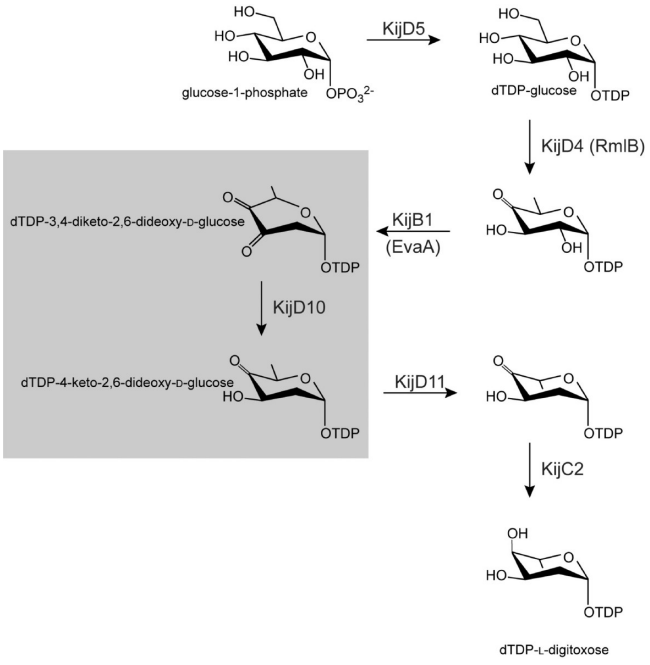


**Scheme 2**

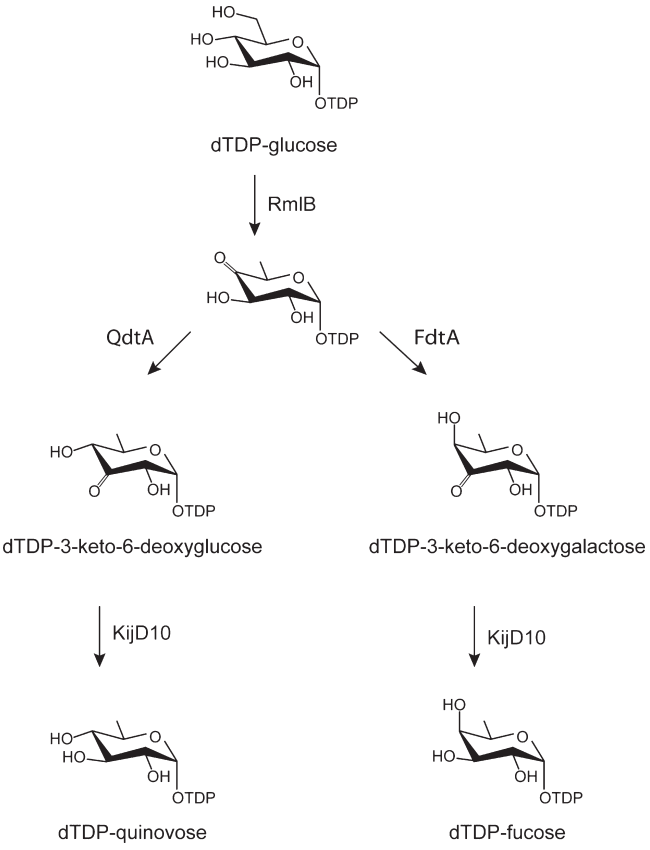


these site-directed mutant proteins were determined. Taken together, these studies provide new molecular details for C-3″-ketoreductases in general.

## MATERIALS AND METHODS

**Cloning, Expression, and Purification.** The *kijd10* gene was amplified via polymerase chain reaction (PCR) from *A. kijaniata* (ATCC 31588) genomic DNA using the forward primer 5′-AAA*CATATG*GAGAATCCGGCGAACGCCAATCCG-3′ and the reverse primer 5′-AAA*CTCGAG*TCAGGGGAAGTAGATGTCGCGC-3′, which added *Nde*I and *Xho*I cloning sites, respectively. Subsequently, the purified PCR product was A-tailed and ligated into the pGEM-T vector (Promega) for screening and sequencing. A pGEM-T-*kijd10* vector construct of the correct sequence was then appropriately digested and ligated into a pET28JT vector[15] for production of protein with a TEV protease cleavable N-terminal hexahistidine tag.

The pET28JT-*kijd10* plasmid was used to transform Rosetta 2 (DE3) *Escherichia coli* cells (Novagen). Cultures were grown in TB medium supplemented with kanamycin and chloramphenicol at 37 °C and subjected to shaking until optical densities of 0.8 were reached at 600 nm. The flasks were then cooled to 24 °C, and cell growth was continued for 20 h. The cells were subsequently induced with 50 $\mu$M IPTG and allowed to express protein at 24 °C for an additional 18 h. KijD10 was purified at 4 °C utilizing Ni-NTA resin (Qiagen) according to standard procedures. Purified protein was then dialyzed against 25 mM Tris (pH 8.0), 200 mM NaCl, and 10% glycerol. The protein preparation was concentrated to approximately 13 mg/mL using an extinction coefficient of 0.94 mL mg$^{-1}$ cm$^{-1}$ at 280 nm and subsequently flash-frozen in liquid nitrogen.

**Activity Assay with dTDP-3,4-diketo-2,6-dideoxy-D-glucose.** To verify that the KijD10 preparation used in this investigation was enzymatically active, reaction mixtures containing 50 mM HEPES (pH 7.5), 0.5 mM dTDP-glucose, 200 $\mu$M NADPH, 10% glycerol, 1 mg/mL 4,6-dehydratase (RmlB), 0.3 mg/mL 2,3-dehydratase (EvaA), and 10 $\mu$g/mL 3-ketoreductase (KijD10) were set up (see Scheme 1). The required 4,6-dehydratase (RmlB) and the 2,3-dehydratase (EvaA) were previously cloned and purified in the laboratory from *E. coli* and *Amycolatopsis orientalis*, respectively. The dTDP-glucose was synthesized according to previously published procedures.[16] The reactions were initiated via the addition of EvaA and were conducted at 25 °C on a Beckman Coulter DU-640 spectrophotometer (Beckman Coulter) for 10 min. Reduction of the C-3″ keto group of the 3,4-diketosugar substrate and the concurrent oxidation of NADPH to NADP$^+$ were monitored by a decrease in absorbance at 340 nm. Control reactions conducted in the absence of any one of the enzymes (RmlB, EvaA, or KijD10) resulted in no decrease in absorbance, thereby indicating that neither NADPH oxidation nor sugar reduction occurred. Importantly, these control experiments demonstrate that NADPH is oxidized only in the presence of KijD10 and its proper dTDP-linked sugar substrate.

**Production of dTDP-Quinovose and dTDP-Fucose.** The KijD10 substrate, dTDP-3,4-diketo-2,6-dideoxy-D-glucose, was stable enough for the activity assays described above, but too unstable to allow for the determination of $k_{cat}$ and $K_m$ values. To test the ability of KijD10 to function on the more stable molecules, dTDP-3-keto-6-deoxyglucose or dTDP-3-keto-6-deoxygalactose, the production of dTDP-quinovose or dTDP-fucose, respectively, was monitored as outlined in Scheme 2. Each reaction mixture contained 0.5 mg/mL KijD10 in 50 mM HEPES (pH 7.5), 5 mM NADPH (Sigma), 1 mg/mL RmlB, and

either 0.5 mg/mL QdtA for dTDP-quinovose or FdtA for dTDP-fucose production. The 3,4-ketoisomerase QdtA or FdtA were previously cloned and purified in the laboratory.[17] The reaction mixtures were incubated at 30 °C for 3 h, after which they were passed through a 10 kDa cutoff filter (Amicon) to remove the enzymes. The filtrates were then diluted 1:9 with water.

Contaminants were removed from the reaction flow-through using an ÄKTA Purifier HPLC system (GE Healthcare) equipped with a Resource-Q 6 mL anion exchange column (GE Healthcare). The column was first equilibrated with water, after which the reaction flow-through was loaded onto it. The column was then washed and eluted with a linear gradient to 50% ammonium acetate (2 M, pH 4.0) over 15 column volumes (CV). The flow rate was 6 mL/min, and the elution was monitored at 267 nm.

The identities of the dTDP-quinovose and dTDP-fucose products were confirmed by ESI mass spectrometry (Mass Spectrometry/Proteomics Facility, University of Wisconsin) and NMR spectroscopy (Nuclear Magnetic Resonance Facility, University of Wisconsin). The ESI mass spectrometry parent ions for both dTDP-quinovose and dTDP-fucose were at $m/z$ 547.1. The observed NMR values were in agreement with those previously determined for dTDP-quinovose or dTDP-fucose.[18] These data clearly demonstrate that KijD10 can turn over either dTDP-3-keto-6-deoxyglucose or dTDP-3-keto-6-deoxygalactose, thus allowing for a detailed kinetic analysis to be conducted on the wild-type and mutant enzymes as described below.

Fractions containing the reduced sugars were pooled and diluted 1:5 with water; the pH was adjusted to 8.0, and the sugars were further purified over the 6 mL Resource-Q column using a linear gradient from 17 to 22% ammonium acetate (2 M, pH 4.0) over 10 CV with a flow rate of 6 mL/min. The fractions containing dTDP-quinovose or dTDP-fucose were pooled and lyophilized until the buffer was completely removed.

**Crystallization of KijD10.** Suitable crystallization conditions were initially surveyed by the hanging drop method of vapor diffusion using a sparse matrix screen developed in the laboratory. Diffraction quality crystals of the N-terminal His-tagged apoenzyme protein at a concentration of 13 mg/mL were grown by mixing in a 1:1 ratio the enzyme solution with 1.0−1.2 M sodium/potassium phosphate and 100 mM CHES (pH 9.0). These crystals belonged to space group $I222$ with one monomer per asymmetric unit and the following unit cell dimensions: $a$ = 72.9 Å, $b$ = 104.8 Å, and $c$ = 144.9 Å.

**Structural Analysis of KijD10.** The initial structure of KijD10 was determined by multiple isomorphous replacement with two heavy atom derivatives. Apoenzyme crystals were soaked in either 10 mM potassium gold cyanide or 6 mM platinum tetrachloride for 4 or 2 days, respectively. Prior to X-ray data collection, these crystals were transferred to a stabilization solution of 1.4 M sodium/potassium phosphate (pH 8.0) and 100 mM NaCl. All X-ray data sets for this initial structural analysis were measured at 4 °C with a Bruker HI-STAR area detector system equipped with Supper mirrors. The X-ray source was Cu Kα radiation from a Rigaku RU200 X-ray generator operated at 50 kV and 90 mA. Two gold and two platinum binding sites were identified with SOLVE.[19] Solvent flattening with RESOLVE[20] generated an interpretable electron density map. A preliminary model of the enzyme was constructed using Coot.[21]

For higher-resolution X-ray data sets, crystals of KijD10 were grown in the presence of either 5 mM $NADP^+$ (binary complex)

**Table 1. X-ray Data Collection Statistics**[a]

| | native data set for MIR phasing | KAuCN | $Pt(CN)_4$ | enzyme·$NADP^+$·dTDP-benzene (closed) | enzyme·$NADP^+$·dTDP-benzene (open) | enzyme·$NADP^+$ | Y186F | K102A | K102E |
|---|---|---|---|---|---|---|---|---|---|
| resolution limits | 44−2.59 | 47−2.59 | 53−2.60 | 60−1.71 | 60−1.80 | 65−1.90 | 65−2.0 | 72−1.91 | 65−2.49 |
| | (2.69−2.59) | (2.69−2.59) | (2.70−2.60) | (1.80−1.71) | (1.90−1.80) | (2.0−1.90) | (2.1−2.0) | (2.01−1.91) | (2.58−2.49) |
| no. of independent reflections | 17190 (1347) | 16832 (1331) | 17242 (1505) | 59618 (8171) | 49314 (6888) | 41479 (5420) | 36599 (4483) | 37962 (4673) | 18970 (1756) |
| completeness (%) | 94.0 (72.6) | 92.3 (72.1) | 94.9 (76.0) | 99.6 (98.2) | 95.2 (89.3) | 94.9 (90.4) | 96.9 (88.8) | 91.1 (73.1) | 96.9 (86.9) |
| redundancy | 2.7 (1.6) | 2.6 (1.4) | 2.7 (1.6) | 4.2 (2.9) | 5.0 (2.4) | 4.3 (2.4) | 4.9 (2.3) | 4.1 (1.4) | 4.0 (1.9) |
| average $I$/average $\sigma(I)$ | 9.6 (4.5) | 7.7 (3.0) | 11.4 (5.2) | 8.3 (1.5) | 13.1 (2.1) | 11.2 (2.9) | 13.5 (3.9) | 12.9 (2.2) | 10.6 (3.2) |
| $R_{sym}$ (%)[b] | 8.3 (16.4) | 10.2 (23.4) | 6.7 (14.0) | 8.1 (64.3) | 8.4 (52.7) | 8.3 (28.4) | 8.2 (20.7) | 6.7 (25.4) | 9.6 (23.8) |

[a] Statistics for the highest-resolution bin are given in parentheses. [b] $R_{sym} = (\Sigma|I - \bar{I}|/I) \times 100$.


dx.doi.org/10.1021/bi200514b |*Biochemistry* 2011, 50, 5905–5917

**Table 2. Refinement Statistics**

| | ternary complex, closed | ternary complex, open | binary complex | Y186F | K102A | K102E |
|---|---|---|---|---|---|---|
| space group | *I*222 | *I*222 | *I*222 | *I*222 | *I*222 | *I*222 |
| unit cell dimensions (Å) | 72.8, 104.1, 145.3 | 73.1, 104.8, 144.5 | 73.3, 104.0, 144.6 | 72.8, 104.2, 145.5 | 73.0, 104.5, 145.0 | 72.4, 103.5, 145.2 |
| resolution limits (Å) | 85−1.71 | 85−1.80 | 84−1.90 | 85−2.0 | 85−1.9 | 84−2.49 |
| *R* factor[a] (overall) (%)/no. of reflections | 20.5/59613 | 20.9/49314 | 19.3/41479 | 19.3/36597 | 20.6/39762 | 19.2/18970 |
| *R* factor (working) (%)/no. of reflections | 20.4/56605 | 20.7/46806 | 19.1/39401 | 19.1/34762 | 20.4/37752 | 18.9/18010 |
| *R* factor (free) (%)/no. of reflections | 23.4/3008 | 24.3/2508 | 22.3/2078 | 23.2/1835 | 24.5/2010 | 25.3/959 |
| no. of protein atoms | 2583 | 2524 | 2500 | 2581 | 2474 | 2478 |
| no. of heteroatoms | 468[b] | 386[c] | 347[d] | 339[e] | 316[f] | 280[g] |
| average *B* value (Å$^2$) | | | | | | |
| protein atoms | 18.9 | 18.5 | 17.3 | 15.9 | 20.3 | 16.6 |
| ligands | 21.3 | 25.5 | 20.6 | 23.5 | 29.4 | 29.4 |
| solvent | 31.6 | 29.4 | 29.7 | 25.2 | 27.5 | 25.9 |
| weighted root-mean-square deviation | | | | | | |
| from ideality | | | | | | |
| bond lengths (Å) | 0.010 | 0.010 | 0.010 | 0.011 | 0.011 | 0.010 |
| bond angles (deg) | 2.4 | 2.3 | 2.3 | 2.4 | 2.3 | 2.3 |
| general planes (Å) | 0.009 | 0.009 | 0.009 | 0.009 | 0.009 | 0.008 |
| Ramachandran statistics (%) | | | | | | |
| core | 92.5 | 92.9 | 92.6 | 91.0 | 92.9 | 90.7 |
| allowed | 7.2 | 7.1 | 7.4 | 8.6 | 7.1 | 9.3 |
| generously allowed | 0.3 | none | none | 0.4 | none | none |

[a] *R* factor = $(\Sigma|F_o - F_c|/\Sigma|F_o|) \times 100$, where $F_o$ is the observed structure factor amplitude and $F_c$ is the calculated structure factor amplitude. [b] These include dTDP-benzene, $NADP^+$, one phosphate, one sodium, two chlorides, one ethylene glycol, and 377 waters. [c] These include dTDP-benzene, $NADP^+$, one phosphate, one sodium, two chlorides, one ethylene glycol, and 295 waters. [d] These include $NADP^+$, one phosphate, one sodium, two chlorides, one ethylene glycol, and 287 waters. [e] These include dTDP-benzene, $NADP^+$, one phosphate, one sodium, two chlorides, and 252 waters. [f] These include two dTDP-benzenes, $NADP^+$, one phosphate, one sodium, one chloride, and 199 waters. [g] These include two dTDP-benzenes, $NADP^+$, one phosphate, one sodium, one chloride, and 163 waters.

or a combination of 5 mM $NADP^+$ and 5 mM dTDP-benzene (ternary complex). Prior to X-ray data collection, single crystals of the binary complex were transferred to a synthetic mother liquor containing 1.4 M sodium/potassium phosphate (pH 8.0), 100 mM HEPPS, 100 mM NaCl, and 10 mM $NADP^+$ for at least 1 h. Crystals of the ternary complex were transferred to a similar synthetic mother liquor containing 10 mM $NADP^+$ and 10 mM dTDP-benzene. Subsequently, these crystals were transferred in five steps to a cryoprotectant solution containing 1.6 M sodium/potassium phosphate (pH 8.0), 200 mM NaCl, 15% ethylene glycol, and 10 mM $NADP^+$ (or 10 mM $NADP^+$ and 10 mM dTDP-benzene in the case of the ternary complex). High-resolution X-ray data sets were collected at 100 K with a Bruker AXS Platinum 135 CCD detector equipped with Montel optics and controlled by the Proteum software suite (Bruker AXS Inc.). These data sets were processed with SAINT version 7.06A (Bruker AXS Inc.) and internally scaled with SADABS version 2005/1 (Bruker AXS Inc.). Relevant X-ray data collection statistics are listed in Table 1. The binary and ternary complex models were constructed using Coot and refined with REFMAC.[22] Refinement statistics are listed in Table 2.

**Production of Site-Directed Mutant Proteins.** The K102A, K102E, K102Q, K102M, and Y186F mutations were introduced using methods identical or similar to those described within the QuikChange site-directed mutagenesis kit (Stratagene). Each mutant protein was expressed and purified in a manner identical to that previously described for the wild-type enzyme. The mutant proteins were dialyzed against 25 mM Tris-HCl (pH 8.0), 200 mM NaCl, and 10% glycerol. Protein concentrations ranged from 12 to 15 mg/mL as measured from the absorbance at 280 nm and using an extinction coefficient of 0.94 mL mg$^{-1}$ cm$^{-1}$. All samples were flash-frozen.

Crystals of the Y186F, K102A, and K102E mutant proteins with bound $NADP^+$ and dTDP-benzene were prepared in a similar manner as previously discussed. X-ray data sets were collected on the CCD detector, and the structures of the mutant proteins were determined by molecular replacement using PHASER.[23] Relevant data collection and model refinement statistics are given in Tables 1 and 2, respectively.

**Determination of Kinetic Constants.** Steady-state kinetic parameters for KijD10 were determined via a spectrophotometric assay. All reaction mixtures contained 50 mM HEPES (pH 7.5), 200 $\mu$M NADPH, 1 mg/mL RmlB, and 0.3 mg/mL FdtA or QdtA (Scheme 2). Additionally, dTDP-glucose was added to final concentrations ranging from 0.025 to 20 mM. Reaction mixtures containing QdtA were run with 2.5 $\mu$g/mL KijD10. Because of substrate inhibition of QdtA with dTDP-glucose concentrations of >0.075 mM, steady-state kinetic parameters could not be determined using the "dTDP-quinovose" assay (Scheme 2). This substrate inhibition was not observed when monitoring the production of dTDP-fucose, however. Consequently, the reported kinetic parameters in Table 3 were determined using dTDP-glucose as the starting material and reacting with RmlB and FdtA. These reactions were conducted with KijD10 concentrations of 1 $\mu$g/mL for the wild-type enzyme, 0.5 mg/mL for the K102E mutant protein, and

**Table 3. Kinetic Parameters**

| protein | $V_{max}$ (mM/min) | $K_m$ (mM), dTDP-linked sugar | $K_m$ (mM), NADPH | $k_{cat}$ ($s^{-1}$), dTDP-linked sugar | $k_{cat}/K_m$ ($M^{-1}s^{-1}$), dTDP-linked sugar |
|---|---|---|---|---|---|
| wild-type | 0.0101 ± 0.0001[a] | 0.1164 ± 0.0044 | 6.31 ± 1.06 | 6.24 ± 0.74 | (5.38 ± 0.06) × $10^4$ |
| Y186F | 0.0116 ± 0.0003 | 0.1180 ± 0.0091 | 10.44 ± 2.73 | 0.716 ± 0.02 | (6.07 ± 0.11) × $10^3$ |
| K102A | ND[b] | ND | ND | ND | ND |
| K102E[c] | 0.0080 ± 0.0006 | 6.3201 ± 1.2001 | –[d] | 0.010 ± 0.003 | 1.56 ± 0.48 |
| K102M | ND | ND | ND | ND | ND |
| K102Q | ND | ND | ND | ND | ND |

[a] Standard errors are reported. [b] Not determined. The rate was too slow to provide an accurate measurement via the spectrophotometric assay that was utilized. [c] Due to spectrophotometer limitations, it was not possible to reach 5 times the $K_m$ for the dTDP-sugar substrate. As a consequence, the reported numbers are all apparent values. [d] Could not be determined because of spectrophotometer limitations.

10 $\mu$g/mL for the Y186F mutant protein. For K102A, K102M, and K102Q, the protein concentration was 1 mg/mL. The reactions were initiated with the addition of FdtA and were conducted at 25 °C on a Beckman Coulter DU-640 spectrophotometer (Beckman Coulter) for 10 min. Reduction of the 3-ketosugar substrate, and concurrent oxidation of NADPH to $NADP^+$, was monitored by a decrease in absorbance at 340 nm. The data were fitted to the equation $v_0 = (V_{max}[S])/(K_M + [S])$. The $k_{cat}$ values were calculated according to the equation $k_{cat} = V_{max}/[E_T]$.

Steady-state kinetic assays for KijD10 with the NADPH cofactor were conducted in a manner similar to that of the assays described above. For these reactions, the dTDP-glucose concentration was held constant at 0.5 mM whereas the NADPH concentrations varied from 5 to 20 $\mu$M. All enzyme concentrations were as listed above. Each reaction for the varied NADPH concentrations was conducted in triplicate, and the rates were averaged and graphed in a double-reciprocal plot. A linear equation fit to the data was used to determine the kinetic parameters. It was not possible to use the Michaelis–Menten equation given above because of limits of the instrumentation.

To verify that the KijD10 substrate did not break down during the course of the reactions outlined above, the following experiments were conducted. Reaction mixtures containing 50 mM HEPES (pH 7.5), 0.5 mM dTDP-glucose, 200 $\mu$M NADPH, 1 mg/mL RmlB, 0.3 mg/mL FdtA, and 1 $\mu$g/mL KijD10 were set up. The reaction mixtures were incubated at 25 °C for up to 10 min. Samples were removed at 0, 3, and 10 min, and the reactions were quenched with HCl added to a final concentration of 0.08 M. Carbon tetrachloride was added to each sample, and after the samples had been mixed and briefly centrifuged, 100 $\mu$L of the aqueous layer was mixed 1:9 with water. All samples were run over an ÄKTA Purifier HPLC system (GE Healthcare) equipped with a 1 mL Resource-Q anion exchange column (GE Healthcare). The samples were loaded onto the column in water and eluted with a linear gradient from 0 to 50% ammonium acetate (2 M, pH 4.0) over 20 CV with a flow rate of 2 mL/min. The presence of dTDP from dTDP-sugar breakdown was monitored at 267 nm. There was no significant change in the peak area corresponding to dTDP, thus indicating that all sugars were stable during the course of the assay.

Note that for the assays described above, the KijD10 substrate was synthesized in situ. This was done out of necessity because of the instability of the substrate. As such, several controls were conducted to confirm that the first two enzymes (RmlB and FdtA) were at saturating concentrations and were not rate-limiting. For one set of controls, either RmlB or FdtA was doubled in concentration while all other conditions were kept identical to those described above. The reactions were monitored for 10 min. No changes in rates were observed for either case, indicating that both enzymes were at saturating concentrations. A second set of controls was run to ensure that the rate of the reaction increased linearly with an increase in KijD10 concentration. For these experiments, the dTDP-glucose concentration was held at 1 mM, while KijD10 concentrations ranged from 0.3 to 2 $\mu$g/mL. All other reaction conditions remained the same. After 10 min, the rates were plotted versus enzyme concentration and yielded a linear plot with an $R^2$ value of 0.9934. Taken together, these experiments demonstrate that KijD10 is, indeed, the limiting enzyme in the assays.

## RESULTS AND DISCUSSION

**Overall Structure of KijD10.** The first structure of KijD10 determined for this study, that of the enzyme complexed with $NADP^+$ and dTDP-benzene, will be termed the "closed" form. The crystals used for the analysis belonged to space group *I*222 with one subunit per asymmetric unit and diffracted to 1.7 Å resolution. There were no breaks in the polypeptide chain backbone from Asn 8 to the C-terminus.

A close-up of the KijD10 subunit is presented in Figure 1a. The N-terminal region, defined by Asn 8–Phe 131, contains a six-stranded parallel $\beta$-sheet flanked on one side by two and on the other by three α-helices (one of which is contributed by the C-terminal domain). The $\beta$-strands range in length from four to seven residues. As expected for a Rossmann fold motif, the $NADP^+$ cofactor extends across the C-terminal region of the $\beta$-sheet. The C-terminal domain, delineated by Leu 132–Pro 332, is dominated by a nine-stranded, mostly antiparallel $\beta$-sheet flanked on one side by three α-helices. Here the $\beta$-strands range in length from six to 10 residues. The dTDP-benzene ligand lies at the interface of the two domains. There are two *cis*-prolines in KijD10. One of these, Pro 103, lies in the active site cleft and belongs to the Glu-Lys-Pro (or EKP) motif that is mostly conserved in enzymes of the GFOR superfamily.[12,13,24–28] In KijD10, this motif resides in a loop connecting the fifth $\beta$-strand to the fifth α-helix of the Rossmann fold. The *cis*-peptide found in GFOR superfamily members is thought to play a crucial role in positioning the preceding lysine residue into the active site cleft, thereby allowing the enzymes to adopt correct transition-state conformations.[29] Interestingly, in Gal80p, which is a transcriptional repressor, there is a *cis*-alanine in the corresponding position.[14] The functional significance of this *cis*-alanine is presently unknown.[14] The other *cis*-proline in KijD10 is the C-terminal residue.

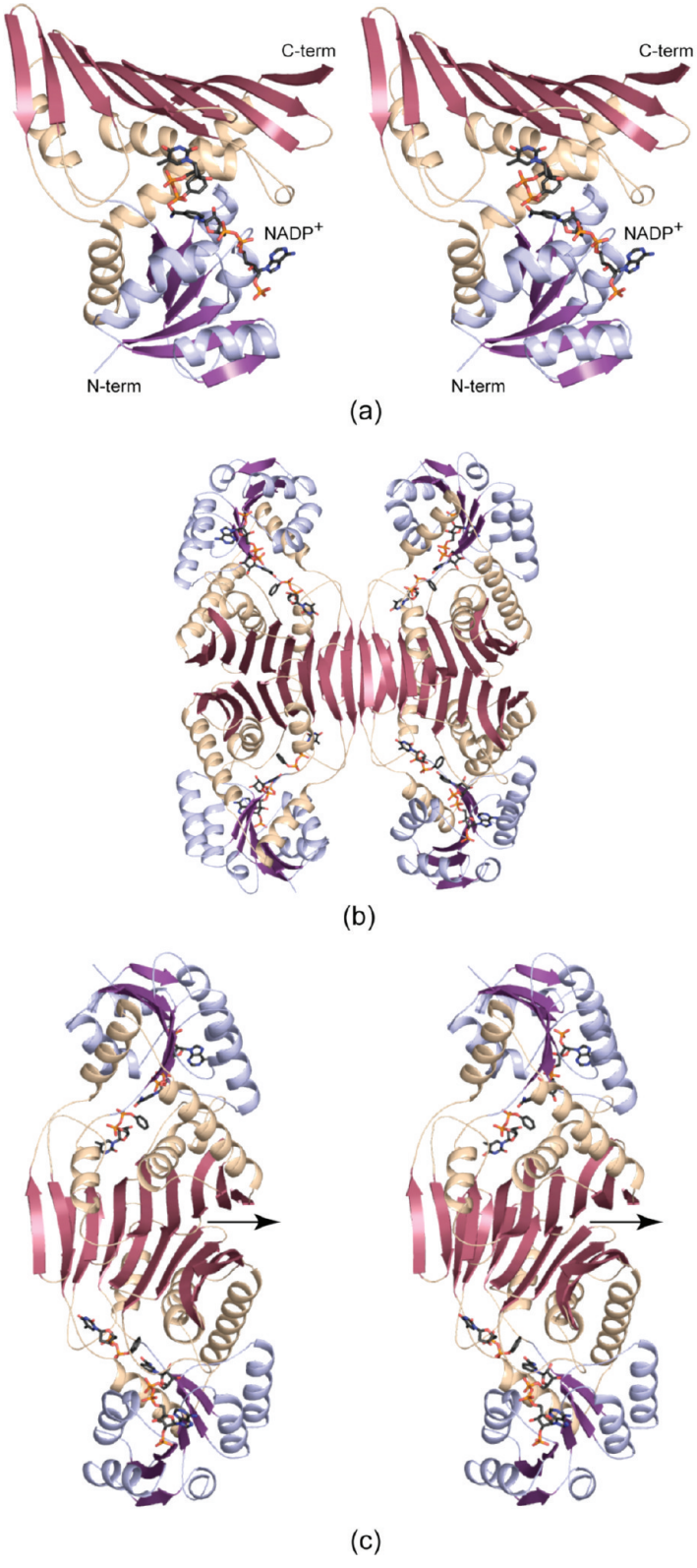


**Figure 1.** Structure of KijD10. The crystals utilized in this investigation contained one molecule per asymmetric unit. (a) Ribbon representation of the KijD10 subunit. The N-terminal domain, which adopts a Rossmann fold, is depicted in light blue and violet, whereas the C-terminal domain is highlighted in wheat and raspberry. The bound ligands are depicted as sticks. (b) Analytical ultracentrifugation experiments indicate that KijD10 behaves as a dimer of dimers. The tetramer demonstrates 222 symmetry. (c) Stereoview of the dimer with the black arrow indicating the position of the molecular 2-fold axis. All figures were prepared with PyMOL.[35]

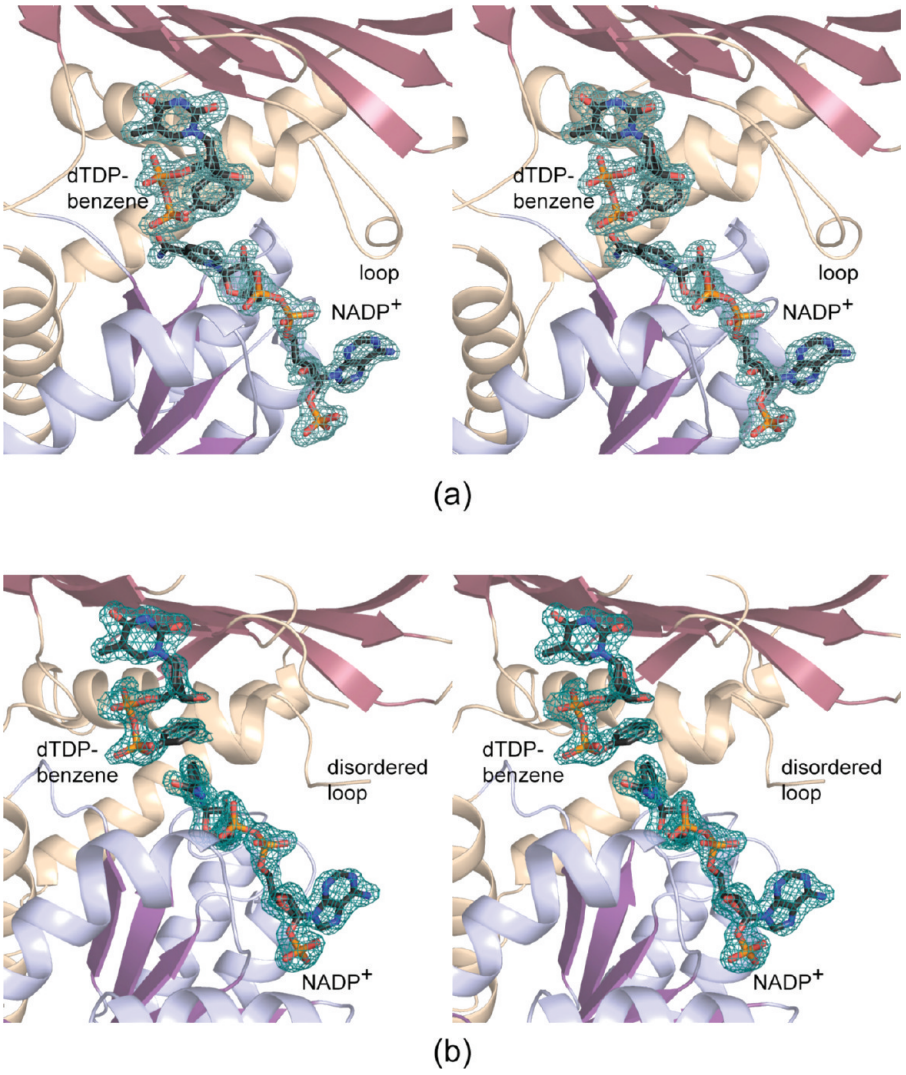


**Figure 2.** Electron density corresponding to the bound ligands, $NADP^+$ and dTDP-benzene. (a and b) Electron densities for the bound ligands in the "closed" and "open" forms of KijD10, respectively. The maps were calculated with coefficients of the form $F_o - F_c$, where $F_o$ was the native structure factor amplitude and $F_c$ was the calculated structure factor amplitude. They were contoured at 2.8$\sigma$ and 2.5$\sigma$, respectively.

Analytical ultracentrifugation experiments indicate that KijD10 alternates between dimers and tetramers, and thus, it can be described as a "dimer of dimers" (unpublished data). Given that there was only one subunit per asymmetric unit, the tetramer necessarily packed in the crystalline lattice with its local dyads coincident to crystallographic 2-fold rotational axes. Shown in Figure 1b is a ribbon representation of the tetramer, which displays 222 symmetry. The buried surface area between the dimers of the tetramer is ~1600 Å$^2$. In this dimer−dimer interface, the eighth $\beta$-strand in the C-terminal domain hydrogen bonds with the symmetry-related $\beta$-strand of another subunit, thereby extending the $\beta$-sheet from nine to 18 strands (Figure 1b). The buried surface area between monomers constituting each dimer is much more extensive (~3200 Å$^2$) as highlighted in Figure 1c. This interface is formed by the mixed $\beta$-sheets of the C-terminal domains and is characterized by numerous hydrogen bonding contacts, some hydrophobic patches, and various water molecules linking one subunit to another. Human glucose-6-phosphate dehydrogenase, another member of the GFOR superfamily, has also been shown to exist in a dimer−tetramer equilibrium that is affected by pH and/or ionic strength.[30] The biological significance of this dimer−tetramer equilibrium is unknown.

Electron density corresponding to the bound ligands in the closed form of KijD10 is presented in Figure 2a. As can be seen, the density is well-ordered and shows that the benzene ring of the substrate analog forms a T-shape stacking interaction with the nicotinamide ring of $NADP^+$. The nicotinamide ring of the dinucleotide adopts the *anti* conformation, as would be expected for an A-side specific enzyme, whereas the adenine ring is in the *syn* orientation. The positions of the adenine rings differ among members of the GFOR superfamily with some adopting the *anti* rather than the *syn* conformation.[13,26,28] Likewise, some GFOR superfamily members are A-side specific such as glucose-fructose oxidoreductase,[12] whereas others are B-side-dependent as in the case of biliverdin IXa reductase.[25]

The active site of KijD10 is quite open with both the deoxythymidine portion of dTDP-benzene and the adenosine moiety of $NADP^+$ solvent-exposed. This is strikingly different from that observed in glucose-fructose oxidoreductase whereby

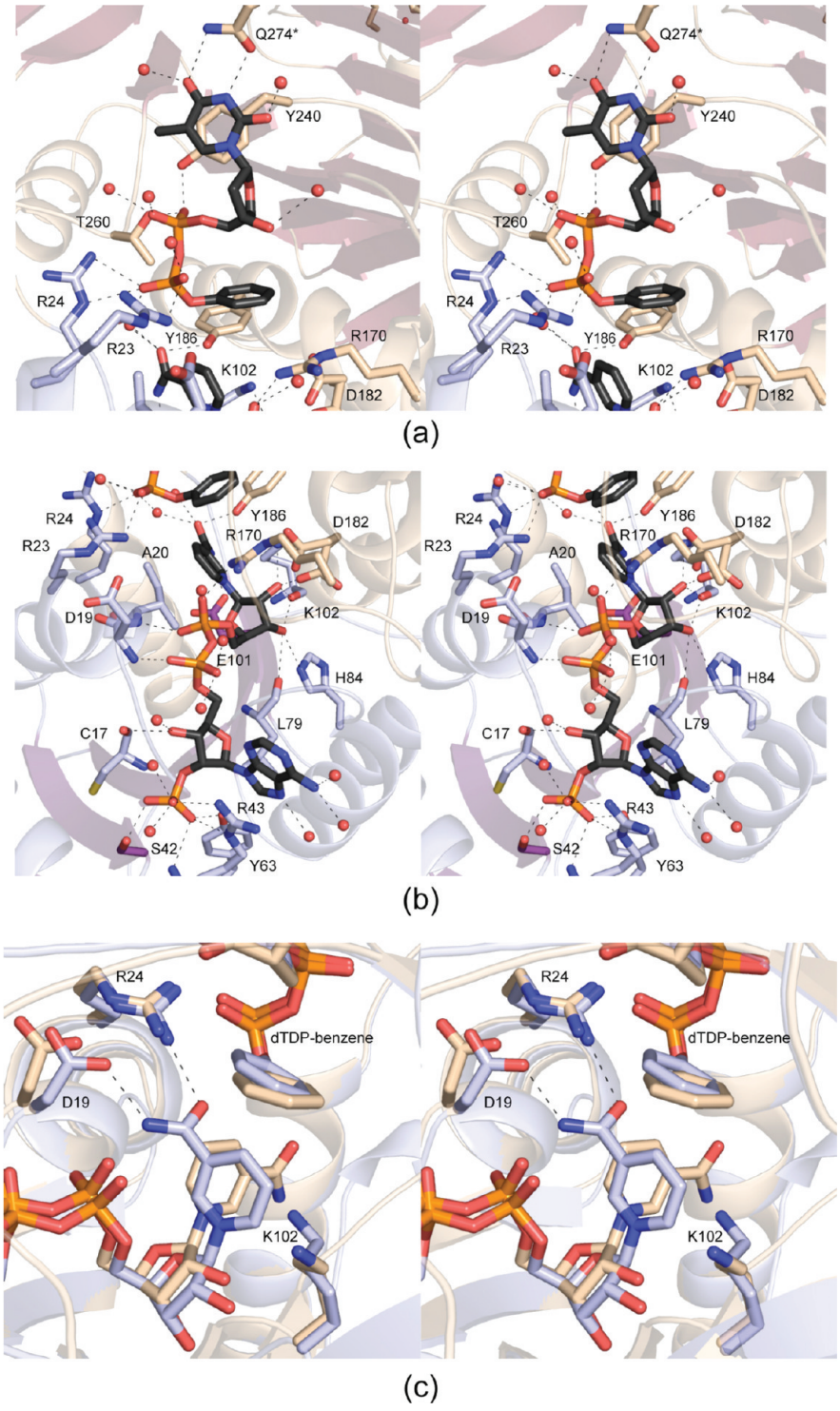


**Figure 3.** Close-up of the KijD10 active site. (a) Region surrounding the dTDP-benzene ligand. Ordered water molecules are represented as spheres. The dashed lines indicate possible hydrogen bonding interactions. (b) Region responsible for positioning the dinucleotide into the active site cleft. (c) Difference in $NADP^+$ binding between the closed and open forms. Those residues belonging to the closed and open versions of KijD10 are colored wheat and light blue, respectively.

the first 23 N-terminal residues close over the active site. Close-ups of the KijD10 active site are presented in Figure 3. The thymine ring of the dTDP-benzene forms a stacking interaction with Tyr 240 and lies within hydrogen bonding distance of Gln 274 from a symmetry-related molecule (Figure 3a). The side chains of Arg 23, Arg 24, Tyr 240, and Thr 260 serve to anchor the pyrophosphoryl group of the substrate analog into the active site cleft. Seven water molecules surround the dTDP-benzene ligand. The dinucleotide cofactor is firmly positioned into the active site by the side chains of Ser 42, Arg 43, Tyr 63, His 84, Glu


dx.doi.org/10.1021/bi200514b |*Biochemistry* 2011, 50, 5905–5917

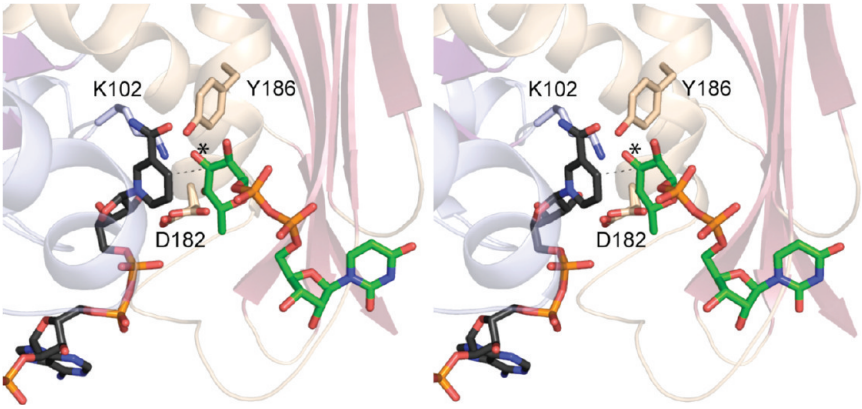


**Figure 4.** Close-up of the binding site for the model of dTDP-3-keto-6-deoxy-D-galactose. The substrate was built into the KijD10 structure on the basis of the observed binding for dTDP-benzene. The dashed line represents the approach of the hydride at C-4 of NADPH to C-3″ (indicated by the asterisk) of the substrate. Asp 182 adopts multiple conformations in the closed model of KijD10.

101, Lys 102, Arg 170, Asp 182, and Tyr 186 (Figure 3b). Additional interactions occur between the dinucleotide and the backbone amide and carbonyls of the polypeptide chain. Numerous ordered water molecules are also associated with the dinucleotide.

The second structure of KijD10 determined in this investigation was again that of the enzyme complexed with $NADP^+$ and dTDP-benzene. Another conformation was observed, however, which will be termed the "open" structure. This second structure was determined to 1.8 Å resolution. Overall, the polypeptide chains for the closed and open models are quite similar, such that their α-carbons superimpose with a root-mean-square deviation of 0.18 Å. The differences arise in the loop defined by Pro 165−Val 175, in the conformation of the nicotinamide ring of $NADP^+$, and in the orientation of Lys 102. In the closed structure, the loop adopts a type II turn (Pro 165−Asp 168) followed by a type I turn (Gln 172−Val 175). It is positioned over the $NADP^+$ binding region (Figure 2a). In the open form, the loop is disordered and the nicotinamide ring of the cofactor adopts the *syn* conformation where its carboxamide group hydrogen bonds to the side chains of Asp 19 and Arg 24 (Figures 2b and 3c). The flipping of the nicotinamide ring is made possible because the side chain of Arg 170, as shown in Figure 3b, moves out of the active site, thereby creating a hole. Lys 102, in the closed structure, forms hydrogen bonds with the C-2 hydroxyl of the nicotinamide ribose, the carbonyl oxygen of Asp 182, and a water molecule. In the open structure, it rotates into the region originally occupied by the carboxamide group of $NADP^+$ (Figure 3c).

To probe the conformational changes that might occur upon dTDP-benzene binding, the third wild-type structure determined in this study to 1.9 Å resolution was that of the enzyme complexed with $NADP^+$ alone. This "binary" structure superimposed upon the open model with a root-mean-square deviation of 0.14 Å, indicating that no major conformational changes occurred. As in the open form, the Lys 164−Gly 177 loop was disordered, and the nicotinamide ring adopted the *syn* conformation.

As described in Materials and Methods, we were able to demonstrate the activity of KijD10 against dTDP-3,4-diketo-2,6-dideoxy-D-glucose. Unfortunately, both the KijD10 substrate and product are unstable compounds (Scheme 1). Consequently, it was not possible to trap these nucleotide-linked sugars in the crystalline lattice or to conduct detailed kinetic studies of KijD10 with its natural substrate. We were able to show, however, that KijD10 can also function on dTDP-3-keto-6-deoxy-D-galactose and dTDP-3-keto-6-deoxy-D-glucose to produce dTDP-fucose and dTDP-quinovose, respectively (Scheme 2). Cocrystallization trials with either 30 mM dTDP-fucose or dTDP-quinovose were unsuccessful, however, in trapping a sugar in the KijD10 active site.

Thus, to gain more insight into the catalytic mechanism of KijD10, we built a model of dTDP-3-keto-6-deoxy-D-galactose into its active site on the basis of the observed binding for dTDP-benzene (Figure 4). In the closed structure, there is an ordered water molecule that lies within hydrogen bonding distance of Lys 102 and Asp 182. It is also positioned 3.1 Å from the nicotinamide ring of $NADP^+$. In our model, the C-4″ hydroxyl group of the hexose is located in this position, and we suggest that the carboxylate of Asp 182 is important for substrate binding. This aspartate belongs to the active site consensus sequence $GGX_3DX_3(Y/H)$ observed in related dehydrogenases and reductases.[31] In glucose-fructose oxidoreductase, for example, the structurally equivalent aspartate is predicted to be a substrate-binding residue.[32] The sugar C-3″ atom of dTDP-3-keto-6-deoxy-D-galactose, which ultimately accepts a hydride from NADPH during the reaction, is located ~3 Å from C-4 of the nicotinamide ring in our model. For catalysis to occur, a proton must be donated to the C-3″ keto group of the hexose, and there are two potential donors located in its vicinity, namely, Lys 102 and Tyr 186. These two residues are not strictly conserved among members of the GFOR superfamily, however. In biliverdin reductase,[25] for example, these residues correspond to Tyr 97 and Ser 170, respectively, whereas in glucose-6-phosphate dehydrogenase[24] they correspond to Lys 171 and His 263, and in dihydrodipicolinate reductase[33] they are replaced by Thr 103 and Thr 170. They are conserved in glucose-fructose oxidoreductase and dihydrodiol dehydrogenase, however, and it is thought that in these enzymes the conserved tyrosine functions as an active site base/acid.[27,32,34] To explore the roles of these two residues in KijD10 catalysis, we initiated a site-directed mutagenesis and kinetic analysis as described below.

**Structures and Functions of the Site-Directed Mutant Proteins.** The first site-directed mutant protein prepared for this study was that in which Tyr 186 was replaced with a phenylalanine residue. In light of the reported kinetic data in the literature on members of the GFOR superfamily, it was anticipated that this mutant protein would be inactive. The $K_m$

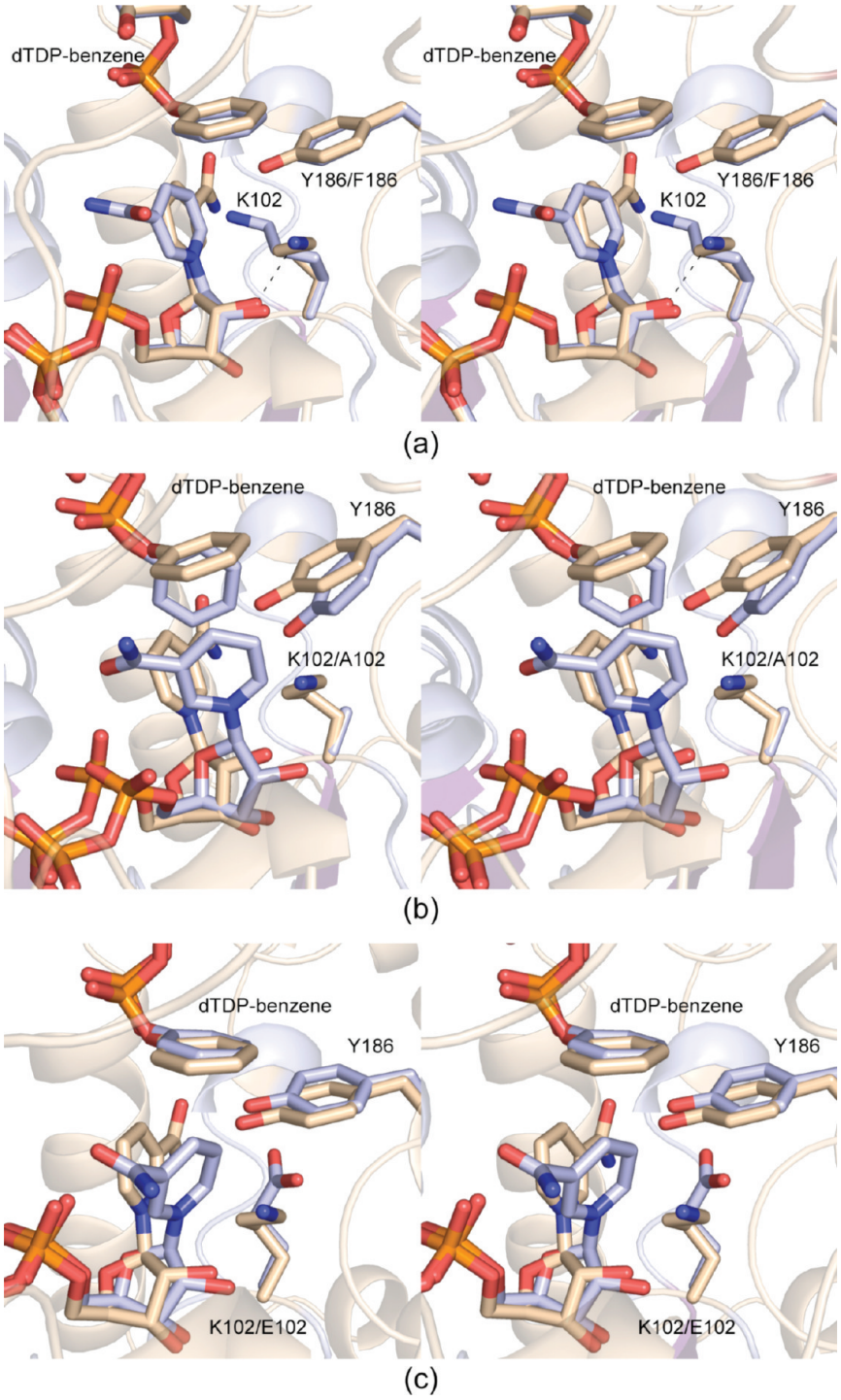


**Figure 5.** Comparison of the active sites for the wild-type and mutant proteins. (a) Close-up of the wild-type protein (closed form, wheat) superimposed upon the Y186F mutant protein (light blue). Similar superpositions of the wild-type enzyme with the K102A and K102E mutant proteins are presented in panels b and c, respectively.

for the dTDP-3-keto-6-deoxy-D-galactose was 0.118 mM, which is the same as that observed for the wild-type enzyme within experimental error (Table 3). Likewise, the $K_m$ for NADPH was relatively unchanged. The $k_{cat}$ for the mutant protein was reduced by approximately 1 order of magnitude. Importantly, the overall catalytic efficiency of the Y186F mutant protein was still quite good at $6.07 \times 10^3$ $M^{-1}$ $s^{-1}$ (Table 3). From these data, it can be concluded that Tyr 186 does not function as the active site acid required to protonate the C-3″ keto oxygen of the dTDP-linked sugar substrate.

The structure of the Y186F protein was subsequently determined to 2.0 Å resolution. Overall, the molecular architecture of the mutant protein is similar to that of the wild-type enzyme such that their α-carbons superimpose with a root-mean-square deviation of 0.10 Å. The electron density for the Pro 165−Val 175 loop was weak, but observable. Likewise, the electron density

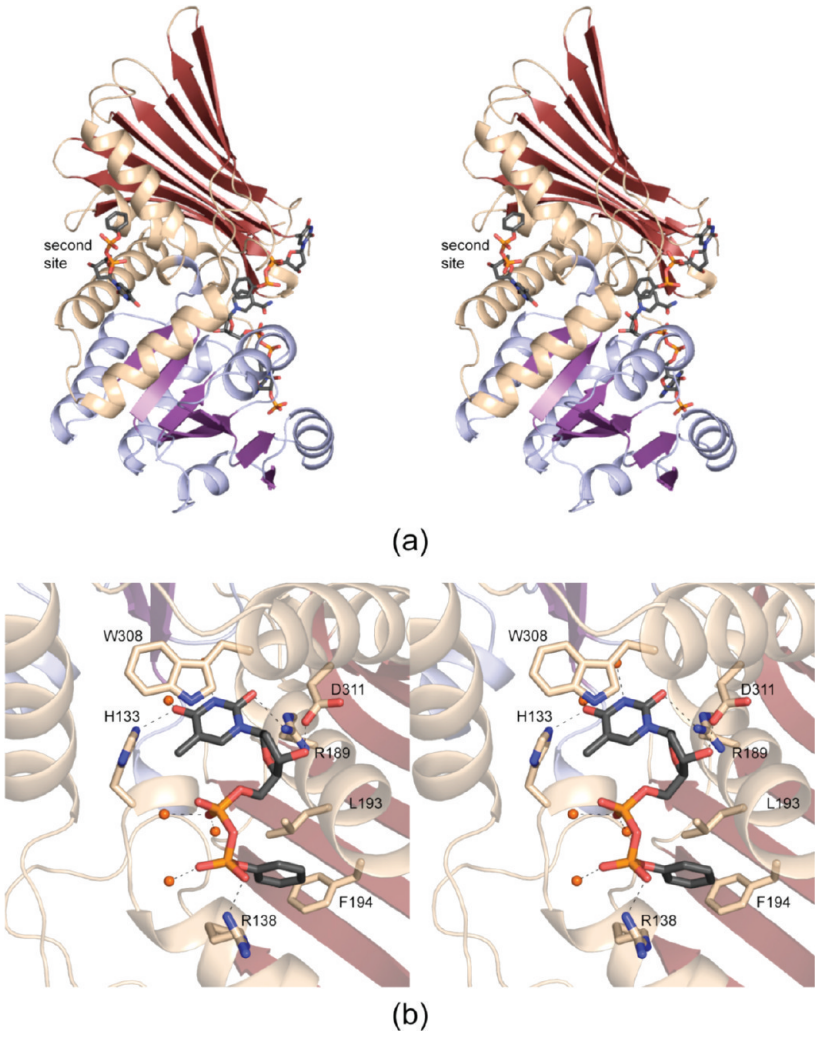


**Figure 6.** Second dTDP-benzene binding site. (a) Position of the second dTDP-benzene binding site, relative to the KijD10 active site. (b) Close-up of the binding interactions between dTDP-benzene and the protein. Potential hydrogen bonding interactions are represented by the dashed lines. Water molecules are depicted as red spheres.

for the nicotinamide of $NADP^+$ was weak, and there was residual $F_o - F_c$ electron density suggesting multiple conformations for the ring. A close-up of the differences between the Y186F and wild-type active sites is presented in Figure 5a. Two major adjustments occur upon substitution of a phenylalanine for a tyrosine. The nicotinamide ring of the $NADP^+$ adopts the *syn* conformation, and the side chain of Lys 102 no longer lies within hydrogen bonding distance of the C-2 hydroxyl of the cofactor ribose. Most likely, the observed reduction in $k_{cat}$ for the Y186F mutant protein results from the conformational flexibility of the nicotinamide ring.

To test the role of Lys 102 in the reaction mechanism of KijD10, we constructed four site-directed mutant proteins: K102A, K102M, K102Q, and K102E. The K102A, K102M, and K102Q mutant proteins were completely inactive under all assay conditions. Interestingly, the K102E retained some activity, but its catalytic efficiency was reduced by more than 4 orders of magnitude from that for the wild-type enzyme. The reaction mechanism of KijD10 requires donation of a proton to the C-3″ keto group of the substrate hexose, and thus, a glutamate at position 102 could possibly fulfill this catalytic role.

Only two of the four site-directed mutant proteins produced X-ray diffraction quality crystals, namely, K102A and K102E. The structure of the K102A mutant protein was determined to 1.9 Å resolution in the open conformation. As in the wild-type open form, the electron density for the loop defined by Pro 163−Val 175 was disordered. The substitution of an alanine for a lysine residue resulted in little overall structural perturbation, however. The α-carbons for the K102A and wild-type proteins superimpose with a root-mean-square deviation of 0.21 Å. A superposition of the active sites for these two proteins is presented in Figure 5b. Removal of the lysine side chain resulted in a shift of both the nicotinamide ring and the ribose in the active site. The nicotinamide flipped into the *syn* conformation. In addition, the benzene moiety of the substrate analog rotated to form a parallel stacking interaction with the nicotinamide ring of $NADP^+$. Crystals of K102E diffracted to only 2.49 Å resolution. Overall, the active site architecture of this mutant protein in the open conformation was similar to that of the wild-type enzyme (Figure 5C). The Pro 163−Val 175 loop was still disordered in the K102E structure, and the electron density corresponding to the nicotinamide ring of $NADP^+$ was weak.


dx.doi.org/10.1021/bi200514b |*Biochemistry* 2011, 50, 5905–5917

Interestingly, in both the K102A and K102E mutant protein structures, a second dTDP-benzene was observed binding to the enzyme as shown in Figure 6a. It is ~17 Å from the active site. The ligand is anchored to the protein via the side chains of His 133, Arg 138, Arg 189, and Asp 311. Leu 193 and Phe 194 provide a hydrophobic pocket for the benzene ring, whereas the side chain of Trp 308 stacks with the thymine ring of the ligand (Figure 6b). The biological significance of this second dTDP-benzene binding site, if any, is unknown at the present time.

In summary, the combined structural and functional analyses of KijD10 reported here represent the first detailed investigation of a ketoreductase that functions on the C-3″ position of a nucleotide-linked sugar. The overall molecular architecture of KijD10 places it into the well-characterized GFOR superfamily. We have demonstrated that in addition to functioning on its natural substrate, KijD10 can also turn over sugars that contain hydroxyl groups at the C-2″ and C-4″ positions, and that it does not discriminate with respect to the orientation of the hydroxyl group at C-4″. Site-directed mutagenesis experiments, kinetic analyses, and structural investigations suggest a mechanism for KijD10 whereby Lys 102 functions as the active site acid required to protonate the C-3″ keto group as a hydride is ultimately transferred from NADPH to the substrate. Finally, a new in vitro enzymatic route for the production of dTDP-quinovose and dTDP-fucose is reported.

### Accession Codes

X-ray coordinates have been deposited in the Protein Data Bank as entries 3RBV, 3RC1, 3RC2, 3RC7, 3RC9, and 3RCB.

## AUTHOR INFORMATION


### Corresponding Author

*E-mail: Hazel_Holden@biochem.wisc.edu. Fax: (608) 262-1319. Phone: (608) 262-4988.



### Funding Sources

This research was supported in part by a National Science Foundation (NSF) grant (MCB-0849274 to H.M.H.) and an NSF predoctoral fellowship (to R.L.K.).


## ACKNOWLEDGMENT

We gratefully acknowledge Professor W. W. Cleland, Dr. James B. Thoden, and Mr. Nathan Bruender for helpful discussions. We thank Mr. Michael J. Palte for help with the NMR data collection and Professor Grover Waldrop and the reviewers for critically reading the manuscript.

## ABBREVIATIONS

CHES, *N*-cyclohexyl-2-aminoethanesulfonic acid; CV, column volume; dTDP-fucose, dTDP-6-deoxygalactose; dTDP-quinovose, dTDP-6-deoxyglucose; IPTG, isopropyl $\beta$-D-thiogalactopyranoside; ESI, electrospray ionization; HEPES, 2-[4-(2-hydroxyethyl)-1-piperazinyl]ethanesulfonic acid; HEPPS, 3-[4-(2-hydroxyethyl)-1-piperazinyl]propanesulfonic acid; $NADP^+$, nicotinamide adenine dinucleotide phosphate (oxidized); NADPH, nicotinamide adenine dinucleotide phosphate (reduced); Ni-NTA, nickel-nitrilotriacetic acid; NMR, nuclear magnetic resonance; PCR, polymerase chain reaction; TB, Terrific Broth; dTDP, thymidine 5′-diphosphate; TEV, tobacco etch virus; Tris, tris(hydroxymethyl)aminomethane.

## REFERENCES


(1) Weymouth-Wilson, A. C. (1997) The role of carbohydrates in biologically active natural products. *Nat. Prod. Rep. 14*, 99–110.

(2) Johnson, D. A., and Liu, H.-w. (1999) *Deoxysugars: Occurrence, genetics, and mechanisms of biosynthesis*, Vol. 3, Elsevier, Amsterdam.

(3) Tomita, F., Tamaoki, T., Shirahata, K., Kasai, M., Morimoto, M., Ohkubo, S., Mineura, K., and Ishii, S. (1980) Novel antitumor antibiotics, tetrocarcins. *J. Antibiot. 33*, 668–670.

(4) Tamaoki, T., Kasai, M., Shirahata, K., and Tomita, F. (1982) Tetrocarcins E1, E2, F and F-1, new antibiotics. Fermentation, isolation and characterization. *J. Antibiot. 35*, 979–984.

(5) Nakajima, H., Sakaguchi, K., Fujiwara, I., Mizuta, M., Tsuruga, M., Magae, J., and Mizuta, N. (2007) Apoptosis and inactivation of the PI3-kinase pathway by tetrocarcin A in breast cancers. *Biochem. Biophys. Res. Commun. 356*, 260–265.

(6) Zhang, H., White-Phillip, J. A., Melancon, C. E., III, Kwon, H. J., Yu, W. L., and Liu, H. W. (2007) Elucidation of the kijanimicin gene cluster: Insights into the biosynthesis of spirotetronate antibiotics and nitrosugars. *J. Am. Chem. Soc. 129*, 14670–14683.

(7) Zielinski, J., Jereczek, E., Sowinski, P., Falkowski, L., Rudowski, A., and Borowski, E. (1979) The structure of a novel sugar component qof polyene macrolide antibiotics: 2,6-Dideoxy-L-ribohexopyranose. *J. Antibiot. 32*, 565–568.

(8) Jakeman, D. L., Bandi, S., Graham, C. L., Reid, T. R., Wentzell, J. R., and Douglas, S. E. (2009) Antimicrobial activities of jadomycin B and structurally related analogues. *Antimicrob. Agents Chemother. 53*, 1245–1247.

(9) Wang, L., White, R. L., and Vining, L. C. (2002) Biosynthesis of the dideoxysugar component of jadomycin B: Genes in the jad cluster of *Streptomyces venezuelae* ISP5230 for L-digitoxose assembly and transfer to the angucycline aglycone. *Microbiology 148*, 1091–1103.

(10) Thibodeaux, C. J., Melancon, C. E., III, and Liu, H. W. (2008) Natural-product sugar biosynthesis and enzymatic glycodiversification. *Angew. Chem., Int. Ed. 47*, 9814–9859.

(11) Holden, H. M., Cook, P. D., and Thoden, J. B. (2010) Biosynthetic enzymes of unusual microbial sugars. *Curr. Opin. Struct. Biol. 20*, 543–550.

(12) Kingston, R. L., Scopes, R. K., and Baker, E. N. (1996) The structure of glucose-fructose oxidoreductase from *Zymomonas mobilis*: An osmoprotective periplasmic enzyme containing non-dissociable NADP. *Structure 4*, 1413–1428.

(13) Thoden, J. B., and Holden, H. M. (2011) Biochemical and structural characterization of WlbA from *Bordetella pertussis* and *Chromobacterium violaceum*: Enzymes required for the biosynthesis of 2,3-diacetamido-2,3-dideoxy-D-mannuronic Acid. *Biochemistry 50*, 1483–1491.

(14) Thoden, J. B., Sellick, C. A., Reece, R. J., and Holden, H. M. (2007) Understanding a transcriptional paradigm at the molecular level. The structure of yeast Gal80p. *J. Biol. Chem. 282*, 1534–1538.

(15) Thoden, J. B., Timson, D. J., Reece, R. J., and Holden, H. M. (2005) Molecular structure of human galactokinase: Implications for Type II galactosemia. *J. Biol. Chem. 280*, 9662–9670.

(16) Hong, L., Zhao, Z., Melancon, C. E., III, Zhang, H., and Liu, H. W. (2008) *In vitro* characterization of the enzymes involved in TDP-D-forosamine biosynthesis in the spinosyn pathway of *Saccharopolyspora spinosa*. *J. Am. Chem. Soc. 130*, 4954–4967.

(17) Davis, M. L., Thoden, J. B., and Holden, H. M. (2007) The X-ray structure of dTDP-4-keto-6-deoxy-D-glucose-3,4-ketoisomerase. *J. Biol. Chem. 282*, 19227–19236.

(18) Elling, L., Rupprath, C., Gunther, N., Romer, U., Verseck, S., Weingarten, P., Drager, G., Kirschning, A., and Piepersberg, W. (2005) An enzyme module system for the synthesis of dTDP-activated deoxysugars from dTMP and sucrose. *ChemBioChem 6*, 1423–1430.

(19) Terwilliger, T. C., and Berendzen, J. (1999) Automated MAD and MIR structure solution. *Acta Crystallogr. D55* (Part 4), 849–861.

(20) Terwilliger, T. C. (2000) Maximum-likelihood density modification. *Acta Crystallogr. D56* (Part 8), 965–972.

(21) Emsley, P., and Cowtan, K. (2004) Coot: Model-building tools for molecular graphics. *Acta Crystallogr. D60*, 2126–2132.

(22) Murshudov, G. N., Vagin, A. A., and Dodson, E. J. (1997) Refinement of macromolecular structures by the maximum-likelihood method. *Acta Crystallogr. D53*, 240–255.

(23) McCoy, A. J., Grosse-Kunstleve, R. W., Adams, P. D., Winn, M. D., Storoni, L. C., and Read, R. J. (2007) Phaser crystallographic software. *J. Appl. Crystallogr. 40*, 658–674.

(24) Rowland, P., Basak, A. K., Gover, S., Levy, H. R., and Adams, M. J. (1994) The three-dimensional structure of glucose 6-phosphate dehydrogenase from *Leuconostoc mesenteroides* refined at 2.0 Å resolution. *Structure 2*, 1073–1087.

(25) Whitby, F. G., Phillips, J. D., Hill, C. P., McCoubrey, W., and Maines, M. D. (2002) Crystal structure of a biliverdin IXα reductase enzyme-cofactor complex. *J. Mol. Biol. 319*, 1199–1210.

(26) Dambe, T. R., Kuhn, A. M., Brossette, T., Giffhorn, F., and Scheidig, A. J. (2006) Crystal structure of NADP(H)-dependent 1,5-anhydro-D-fructose reductase from *Sinorhizobium morelense* at 2.2 Å resolution: Construction of a NADH-accepting mutant and its application in rare sugar synthesis. *Biochemistry 45*, 10030–10042.

(27) Carbone, V., Endo, S., Sumii, R., Chung, R. P., Matsunaga, T., Hara, A., and El-Kabbani, O. (2008) Structures of dimeric dihydrodiol dehydrogenase apoenzyme and inhibitor complex: Probing the subunit interface with site-directed mutagenesis. *Proteins 70*, 176–187.

(28) Thoden, J. B., and Holden, H. M. (2010) Structural and functional studies of WlbA: A dehydrogenase involved in the biosynthesis of 2,3-diacetamido-2,3-dideoxy-D-mannuronic acid. *Biochemistry 49*, 7939–7948.

(29) Vought, V., Ciccone, T., Davino, M. H., Fairbairn, L., Lin, Y., Cosgrove, M. S., Adams, M. J., and Levy, H. R. (2000) Delineation of the roles of amino acids involved in the catalytic functions of *Leuconostoc mesenteroides* glucose 6-phosphate dehydrogenase. *Biochemistry 39*, 15012–15021.

(30) Cohen, P., and Rosemeyer, M. A. (1969) Subunit interactions of glucose-6-phosphate dehydrogenase from human erythrocytes. *Eur. J. Biochem. 8*, 8–15.

(31) Carbone, V., Hara, A., and El-Kabbani, O. (2008) Structural and functional features of dimeric dihydrodiol dehydrogenase. *Cell. Mol. Life Sci. 65*, 1464–1474.

(32) Nurizzo, D., Halbig, D., Sprenger, G. A., and Baker, E. N. (2001) Crystal structures of the precursor form of glucose-fructose oxidoreductase from *Zymomonas mobilis* and its complexes with bound ligands. *Biochemistry 40*, 13857–13867.

(33) Cirilli, M., Zheng, R., Scapin, G., and Blanchard, J. S. (2003) The three-dimensional structures of the *Mycobacterium tuberculosis* dihydrodipicolinate reductase-NADH-2,6-PDC and -NADPH-2,6-PDC complexes. Structural and mutagenic analysis of relaxed nucleotide specificity. *Biochemistry 42*, 10644–10650.

(34) Asada, Y., Aoki, S., Ishikura, S., Usami, N., and Hara, A. (2000) Roles of His-79 and Tyr-180 of D-xylose/dihydrodiol dehydrogenase in catalytic function. *Biochem. Biophys. Res. Commun. 278*, 333–337.

(35) DeLano, W. L. (2002) *The PyMOL Molecular Graphics System*. DeLano Scientific, San Carlos, CA.